Journal of Thermal Stresses, 24:121–140, 2001

0149-5739/01 $12.00 + .00

COUPLED THERMOMECHANICAL WAVES IN HYPERBOLIC THERMOELASTICITY

D. V. Strunin
Department of Mathematics and Computing
University of Southern Queensland
Australia

R. V. N. Melnik
CSIRO Mathematical and Information Sciences
Macquarie University Campus
North Ryde, Australia

A. J. Roberts
Department of Mathematics and Computing
University of Southern Queensland
Australia

Using models incorporating a thermal relaxation time (hyperbolic models), we study the properties of spatially periodic thermoelastic waves propagating in an infinite rod. Analyzing the Lord–Schulman and Green–Lindsay linear models, we reveal dependencies of decay rates and frequency shifts of temperature and displacement upon the wave number for the case of weak thermoelastic coupling. We explore numerically a general nonlinear hyperbolic model, describing the time evolution of initially sinusoidal distributions of displacement and temperature. Mechanisms of nonlinear interaction between thermal and mechanical fields are qualitatively analyzed. It is demonstrated that larger relaxation times may provide smoother temperature profiles at an intermediate stage of the dynamics.

Keywords: coupled thermomechanical fields, hyperbolic thermoelasticity, thermal relaxation time

Received 3 January 2000; accepted 30 June 2000.

This research was supported by an Australian Research Council Grant. Support of CSIRO Mathematical and Information Sciences in providing a travel grant to present a part of this work at the IX Computational Techniques and Applications Conference (Canberra, September 1999) is gratefully acknowledged. Finally, we thank anonymous referees for their comments.

Address correspondence to Dr. Roderick V. N. Melnik, CSIRO Mathematical and Information Sciences, Macquarie University, North Ryde NSW 2113, Australia. E-mail: Roderick.Melnik@cmis.csiro.au

The classical Fourier law of heat conduction and consequent mathematical models constructed on the basis of parabolic partial differential equations (PDEs) provide good approximations for the description of temperature dynamics in a wide range of engineering applications. However, this approach assumes an instantaneous propagation of thermal disturbances to infinitely remote regions. This assumption is physically unrealistic [1] and, in a number of practically important situations, may lead to an inadequate description of heat conduction [2–10] (see also references therein).

A finite speed of thermal disturbances can be taken into account by using models with a thermal relaxation time. These models are based on hyperbolic-type equations for temperature and are closely connected with the theories of *second sound*, which view heat propagation as a wavelike phenomenon.

The literature dedicated to hyperbolic thermoelastic models is quite large, and its detailed review can be found in [2, 5]. The majority of the work in this field has been devoted to various aspects of linear models with a few noticeable exceptions where the nonlinear influence of temperature on thermomechanical field was analyzed (see [3, 4, 6, 9, 11, 12] and references therein).

Despite the extensive research in hyperbolic thermoelasticity carried out during past decades, there remain some important issues for further investigation. Two of them are pursued in the present article. First, by an appropriate modification of the spectral analysis performed in [13], we investigate the spectra of decay rates and frequency shifts of temperature and displacement in a thermoelastic rod using two classical linear models of hyperbolic thermoelasticity. Second, we study numerically the effects of the nonlinearity and relaxation time with a general nonlinear model. Most of the contributions to the study of nonlinear models have concentrated on important theoretical issues, such as existence and uniqueness of solutions, and on identifying the conditions leading to smooth or singular solutions. Only a few papers report numerical results showing distributions of displacement and temperature in a nonlinear thermoelastic body [14, 15]. Using simple sinusoidal waves generated initially in a rod, we demonstrate important effects of the relaxation time and nonlinear interaction between thermal and mechanical fields.

It is well known (see, e.g., [16, 17]) that the nonlinear equation for a longitudinal displacement u in an elastic bar $\partial^2 u/\partial t^2 = \partial/\partial x[\sigma(\partial u/\partial x)]$ (σ is the $\partial u/\partial x$-dependent stress) may lead to a singular solution even for smooth initial data. However, in the case of coupled thermoelasticity the formation of singularities may be suppressed by the dissipative mechanism of heat conduction [18]. On the other hand, if the initial amplitudes of displacement and temperature are sufficiently large, the opposite situation occurs where the damping through heat conduction is not strong enough to guarantee a smooth solution. In this case the role of thermal relaxation increases to a great extent because this factor is the most important for rapidly changing temperature fields.

In the literature addressing *linear* theories with relaxation time, most attention is given to the models formulated by Lord and Schulman (LS) [19] and Green and Lindsay (GL) [20]. Both models are encompassed by a single system of equations

that is written here for the case of a homogeneous isotropic medium:

$$\begin{cases} \rho \dfrac{\partial^2 \mathbf{u}}{\partial t^2} - \mu \Delta \mathbf{u} - (\lambda + \mu) \nabla \operatorname{div} \mathbf{u} - \beta \left(1 + t_1 \dfrac{\partial}{\partial t}\right) \nabla \theta = 0 \\ \rho c (t_2 + t_0) \dfrac{\partial^2 \theta}{\partial t^2} + \rho c \dfrac{\partial \theta}{\partial t} - K \Delta \theta - \beta T_0 \operatorname{div} \left(\dfrac{\partial \mathbf{u}}{\partial t} + t_0 \dfrac{\partial^2 \mathbf{u}}{\partial t^2} \right) = 0 \end{cases} \tag{1}$$

where t_0, t_1, and t_2 are the thermal relaxation times, ρ is the density of the material, μ and λ are Lamé coefficients, K is the coefficient of heat conduction, $\tilde{\beta} = -\beta \equiv (3\lambda + 2\mu)\alpha_T$ is the coupling (thermal pressure) coefficient, α_T is the coefficient of thermal expansion, and T_0 is the reference temperature. The LS model follows from Eq. (1) by setting $t_1 = t_2 = 0$ and the GL model by setting $t_0 = 0$.

The linear hyperbolic models such as Eq. (1) have been studied intensively [13, 21–24]. Recently Suh and Burger [13] presented a spectral analysis of Eq. (1), performed in the spirit of Nowacki [25]. They considered a harmonic plane wave and derived a characteristic equation involving wave number k and frequency ω. The equation can be resolved in two ways, one leading to a result in the form of a function $k = k(\omega)$ and the other leading to a result in the form $\omega = \omega(k)$. In [13] the former approach was used and the resultant wave number k was complex. Thus, the Fourier mode $\exp(ikx)$ grows infinitely as $x \to \pm\infty$ depending on the sign of k.

This makes the approach used in [13] unsuitable for a study of the physically important dynamics of localized disturbances of the trivial state $\mathbf{u} \equiv 0$, $\theta \equiv 0$. The study reduces to the analysis of the time behavior of components of Fourier integrals representing the disturbances. As long as $\exp(ikx)$ represents the Fourier mode, it should involve a real wave number. We address this issue in the second section of the present article, where we focus on how the frequencies and decay rates depend on k.

A nonlinear generalization of the model (1) is written as

$$\begin{cases} \rho \dfrac{\partial^2 \mathbf{u}}{\partial t^2} - \mu \Delta \mathbf{u} - (\lambda + \mu) \nabla \operatorname{div} \mathbf{u} - \beta \left(1 + t_1 \dfrac{\partial}{\partial t}\right) \nabla \theta = \mathbf{F}_1(\mathbf{u}, \theta) \\ \rho c (t_2 + t_0) \dfrac{\partial^2 \theta}{\partial t^2} + \rho c \dfrac{\partial \theta}{\partial t} - K \Delta \theta - \beta T_0 \operatorname{div} \left(\dfrac{\partial \mathbf{u}}{\partial t} + t_0 \dfrac{\partial^2 \mathbf{u}}{\partial t^2} \right) = F_2(\mathbf{u}, \theta) \end{cases} \tag{2}$$

where the nonlinear operators $\mathbf{F}_1$ and F_2 are determined by the constitutive relations that couple stresses, deformation gradients (strains), temperature, and heat fluxes. In the third section of the present article we explore model (2) corresponding to the GL model with the operators $\mathbf{F}_1$ and F_2 derived by Maugin and his collaborators (see [14] and references therein).

The recent works [14] and [15] are dedicated to one-dimensional nonlinear thermoelasticity without a relaxation time. The boundary condition for displacement was chosen in these works in the form of sinusoidal oscillations. The boundary condition for temperature was chosen in [14] in the form of oscillations fitted to displacement in a special way in order to provide a traveling wave solution. Note that such a setting was viewed by the authors of [14] as a problem about harmonic

waves with no thermal boundary condition. We believe, however, that this interpretation just reflects the fact that an *arbitrary* thermal boundary condition cannot be imposed once the form of the solution is stipulated. In [15] the thermal boundary condition had the form of a proportionality between the heat flux and temperature.

Our choice in this article is to consider spatially periodic waves in a rod. There are several reasons in favor of such a consideration. In the linear case the spatially periodic (harmonic) waves play a key role in the description of the behavior of arbitrarily shaped initially localized disturbances of temperature and displacements. Indeed, due to the linear nature of the model, each Fourier mode can be studied separately from the others; therefore, in this situation, it suffices to consider a harmonic wave with an arbitrary wave number. In the nonlinear case, (thermo-) elastic rods have become an important nontrivial object of studies since the time of classical works on nonlinear elasticity [26]. At present, dynamic rod models are used in many important applications ranging from classical mechanics [27] to the study of basic properties of DNA and bimolecular structures [28]. In this article we limit our consideration to the infinite rod mainly because such an object has no boundary (although, from a mathematical point of view, it can be said that it is subjected to a periodic boundary condition). In this view, it presents a convenient case for the theoretical study of the dynamics free from external influences [29]. It is assumed that in describing the unstressed shape of the rod the energy penalty in deviating from that unstressed shape can be defined according to the standard procedures [30]; we will not consider these issues here.

LINEAR MODELS: SPECTRAL ANALYSIS

In this section we consider the evolution of small disturbances of displacement and temperature. Being small, these obey the linear equations (1). In contrast to the case considered in [13], we assume the wave number k to be real.

We start our spectral analysis with the LS model before examining the GL model:

$$\begin{cases} \rho\dfrac{\partial^2 u}{\partial t^2} - (\lambda+2\mu)\dfrac{\partial^2 u}{\partial x^2} - \beta\dfrac{\partial \theta}{\partial x} = 0 \\ \rho c t_0 \dfrac{\partial^2 \theta}{\partial t^2} - t_0 T_0 \beta \dfrac{\partial^3 u}{\partial t^2 \partial x} + \rho c \dfrac{\partial \theta}{\partial t} - T_0 \beta \dfrac{\partial^2 u}{\partial x \partial t} - K\dfrac{\partial^2 \theta}{\partial x^2} = 0 \end{cases} . \tag{3}$$

Nondimensionalizing with respect to the scales

$$\bar{u} = \frac{K}{c\sqrt{\rho(\lambda+2\mu)}} \qquad \bar{\theta} = T_0 \qquad \bar{x} = \frac{K}{c\sqrt{\rho(\lambda+2\mu)}} \qquad \bar{t} = \frac{K}{c(\lambda+2\mu)} \tag{4}$$

and defining nondimensional parameters

$$\tau = \frac{t_0 c(\lambda+2\mu)}{K} \qquad \beta_1 = \frac{\beta T_0}{\lambda+2\mu} \qquad a = \frac{\beta}{\rho c} \tag{5}$$

we transform model (3) into the form

$$\begin{cases} \dfrac{\partial^2 u}{\partial t^2} - \dfrac{\partial^2 u}{\partial x^2} - \beta_1 \dfrac{\partial \theta}{\partial x} = 0 \\ \tau \dfrac{\partial^2 \theta}{\partial t^2} - \tau a \dfrac{\partial^3 u}{\partial t^2 \partial x} + \dfrac{\partial \theta}{\partial t} - a \dfrac{\partial u}{\partial x \partial t} - \dfrac{\partial^2 \theta}{\partial x^2} = 0 \end{cases} \tag{6}$$

For simplicity, hereafter we use the same notation for the dimensionless quantities as we used earlier for the dimensional quantities.

Once the problem is linear it is sufficient to consider the harmonic disturbances

$$u = U \exp(\omega t + ikx) \qquad \theta = \Theta \exp(\omega t + ikx) \tag{7}$$

Inserting Eq. (7) into model (6) we get the homogeneous system of algebraic equations for their amplitudes, U and Θ.

$$\begin{cases} (\omega^2 + k^2)U - ik\beta_1 \Theta = 0 \\ (-ak\omega i - a\tau\omega^2 ki)U + (\tau\omega^2 + \omega + k^2)\Theta = 0 \end{cases} \tag{8}$$

Equation (8) has a nontrivial solution only if ω satisfies the characteristic equation

$$\tau\omega^4 + \omega^3 + (\tau + 1 + \beta_1 a\tau)k^2\omega^2 + (1 + \beta_1 a)k^2\omega + k^4 = 0 \tag{9}$$

First we investigate under what conditions we may obtain nondecaying dynamics. We assume that the values of the constants are such that the real part of ω is zero. Substituting $\omega = i\omega_1$, where ω_1 is the imaginary part of ω, into Eq. (9) yields

$$\tau\omega_1^4 - i\omega_1^3 - (\tau + 1 + \beta_1 a\tau)k^2\omega^2 + (1 + \beta_1 a)k^2 i\omega_1 + k^4 = 0 \tag{10}$$

Equating the imaginary and real parts of Eq. (10) to zero we get

$$\omega_1^2 = (1 + \beta_1 a)k^2 \qquad \tau\omega_1^4 - (\tau + 1 + \beta_1 a\tau)k^2\omega_1^2 + k^4 = 0 \tag{11}$$

Now, substituting the first equality into the second and making simple rearrangements we obtain

$$a\beta_1 = 0 \tag{12}$$

In view of Eqs. (5) this relation is equivalent to $\beta = 0$, which means that displacement and temperature are decoupled from each other, that is, $a = \beta_1 = 0$. In this case, the dispersion relation, in accord with Eqs. (11), writes

$$\omega = \pm ik \tag{13}$$

Hence, the system (8) is satisfied by arbitrary U and $\Theta = 0$. This solution represents the usual elastic waves.

Now we take into account the coupling and assume the parameter β to be small enough so that $a\beta_1 \ll 1$. Taking into account that the parameters a and β_1 enter the characteristic equation (9) only in combination $a\beta_1$, we seek its solution as an expansion in the small parameter $p = a\beta_1$ about the solution (13):

$$\omega = \pm i(k + \alpha_i p + O(p^2)) + \alpha_r p + O(p^2) \tag{14}$$

where α_i, α_r are real constants. Substituting Eq. (14) into Eq. (9) and equating to zero the real and imaginary parts of the linear terms in a we obtain a pair of linear equations for α_i and α_r:

$$\begin{cases} (\tau - 1)2k^3\alpha_i - 2k^2\alpha_r = \tau k^4 \\ -2k^2\alpha_i + (1 - \tau)2k^3\alpha_r = -k^3 \end{cases} \tag{15}$$

The solution of Eqs. (15) is

$$\alpha_i = \frac{\tau k[k^2(\tau - 1)^2 + 1] - k}{2(\tau - 1)[k^2(\tau - 1)^2 + 1]} \qquad \alpha_r = -\frac{k^2}{2k^2(\tau - 1)^2 + 2} \leq 0$$

The nonpositiveness of α_r implies that both temperature and displacement decay. This vividly demonstrates the damping effect (via the coupling constant β) of the thermal field on the elastic wave. To illustrate the dependencies of α_i and α_r with k we use the parameters typical for steel [23]:

$$\tilde{\beta} = 3.34 \times 10^4 \text{ kg/K/cm/s}^2 \qquad \lambda + 2\mu = 1.99 \times 10^9 \text{ kg/cm/s}^2$$
$$\rho = 7.82 \times 10^{-3} \text{ kg/cm}^3 \qquad c = 4.61 \times 10^6 \text{ cm}^2/\text{K/s}^2$$
$$K = 1.7 \times 10^3 \text{ kg·cm/K/s}^3$$

The typical relaxation time for metals is, by the order of magnitude [2],

$$t_0 = 10^{-15} - 10^{-13} \text{ s}$$

Substituting these values into model (5) gives $a = -0.926$, $\beta_1 = -5.035 \times 10^{-3}$, and $\tau = 0.005 - 0.5$. We observe that for this material the parameter $p = a\beta_1$ is small indeed.

The plot α_r versus k is shown in Figure 1, which demonstrates that short waves decay at the same rate whereas long waves decay slowly with the decay rate going to zero in the limit $k \to 0$. Specifically, we have, for the long waves, $\alpha_r \sim -k^2/2$ as $k \to 0$ and, for the short waves, $\alpha_r \sim -1/[2(\tau - 1)^2]$ as $k \to \infty$. The respective asymptotics of the frequency shift α_i (see Figure 1) are $\alpha_i \sim k/2$ as $k \to 0$ and $\alpha_i \sim -\tau k/2(1 - \tau)$, as $k \to \infty$.

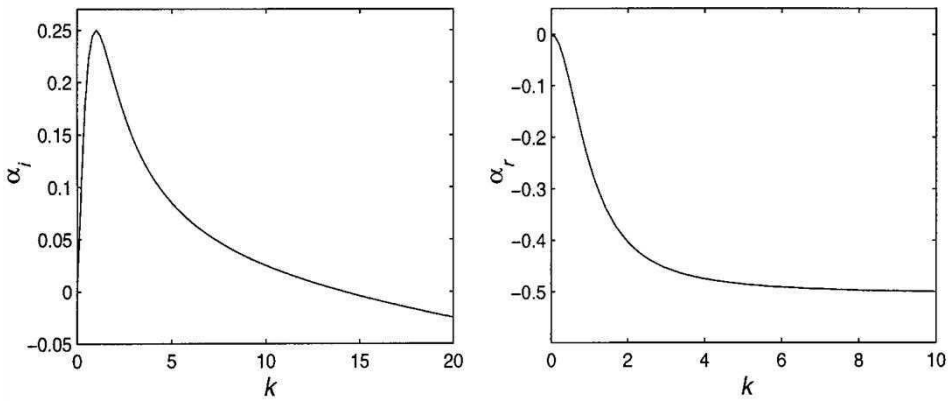

Figure 1. Frequency α_i and decay rate α_r in the LS model (6) with $\tau = 0.005$.

Within the GL model the linear dynamics is described by the system

$$\begin{cases} \dfrac{\partial^2 u}{\partial t^2} - \dfrac{\partial^2 u}{\partial x^2} - \beta_1 \dfrac{\partial \theta}{\partial x} - \beta_1 \tau_1 \dfrac{\partial^2 \theta}{\partial x \partial t} = 0 \\ \tau_2 \dfrac{\partial^2 \theta}{\partial t^2} + \dfrac{\partial \theta}{\partial t} - a \dfrac{\partial u}{\partial x \partial t} - \dfrac{\partial^2 \theta}{\partial x^2} = 0 \end{cases} \tag{16}$$

where

$$\tau_1 = \frac{t_1 c(\lambda + 2\mu)}{K} \qquad \tau_2 = \frac{t_2 c(\lambda + 2\mu)}{K}$$

The characteristic equation in this case has the form

$$\tau_2 \omega^4 + \omega^3 + (\tau_2 + 1 + \beta_1 a \tau_1) k^2 \omega^2 + (1 + \beta_1 a) k^2 \omega + k^4 = 0 \tag{17}$$

As in the previous case we start from the assumption that the parameter values ensure that the real part of ω is zero. This leads to a relation

$$\alpha \beta_1 [(\tau_2 - \tau_1)(1 + a\beta_1) - 1] = 0 \tag{18}$$

Green and Lindsay [20] presented thermodynamical arguments leading to the inequality $\tau_1 \geq \tau_2$. Consequently, since $a\beta_1 \geq 0$, the combination in the square brackets is strictly negative and thus Eq. (18) can be met only if $a\beta_1 = 0$, which corresponds to decoupled fields. Taking the coupling into account by assuming $a\beta_1$

to be a small positive value, we again seek the frequency in the form (14). This leads to

$$\alpha_{\mathrm{i}} = \frac{\tau_1 k[k^2(\tau_2-1)^2+1] - k(1+\tau_1-\tau_2)}{2(\tau_2-1)[k^2(\tau_2-1)^2+1]} \qquad \alpha_{\mathrm{r}} = -\frac{k^2(1+\tau_1-\tau_2)}{2k^2(\tau_2-1)^2+2} \leq 0$$

The value α_{r} is nonpositive and, consequently, temperature and displacement exponentially decay. The dependencies of α_{i} and α_{r} versus k are illustrated in Figure 2. It is easy to write out the asymptotics $\alpha_{\mathrm{r}} \sim -k^2(1+\tau_1-\tau_2)/2$ as $k \to 0$, $\alpha_{\mathrm{r}} \sim -(1+\tau_1-\tau_2)/[2(\tau-1)^2]$ as $k \to \infty$; and $\alpha_{\mathrm{i}} \sim \mathrm{k}/2$ as $k \to 0$, $\alpha_{\mathrm{i}} \sim -\tau_1 k/2/(1-\tau_2)$ as $k \to \infty$.

It is worth remarking that in the particular case $\tau = \tau_1 = \tau_2$ the frequencies and decay rates obtained with the LS and GL models coincide with each other.

NONLINEAR MODEL: NUMERICAL EXPERIMENTS

When disturbances are not small one has to allow for nonlinear effects. In this section we study a nonlinear model obtained by a superposition of the linear GL hyperbolic model and the nonlinear mono-mode model [14] (see details therein):

$$\begin{cases} \dfrac{\partial^2 u}{\partial t^2} - \dfrac{\partial^2 u}{\partial x^2}\left(1 + 2\gamma\dfrac{\partial u}{\partial x} + 3\delta\left(\dfrac{\partial u}{\partial x}\right)^2\right) - \beta_1\dfrac{\partial \theta}{\partial x} - \beta_1\tau_1\dfrac{\partial^2\theta}{\partial x \partial t} - \beta_2\dfrac{\partial}{\partial x}\left(\dfrac{\partial u}{\partial x}\theta\right) = 0 \\ \tau_2\dfrac{\partial^2\theta}{\partial t^2} + \dfrac{\partial}{\partial t}\left(\theta - a\dfrac{\partial u}{\partial x} - \dfrac{1}{2}b\left(\dfrac{\partial u}{\partial x}\right)^2\right) - \dfrac{\partial}{\partial x}\left(\left(1+\alpha\dfrac{\partial u}{\partial x}\right)\dfrac{\partial\theta}{\partial x}\right) = 0 \end{cases} \tag{19}$$

where α, γ, δ, β_2, and b are constants.

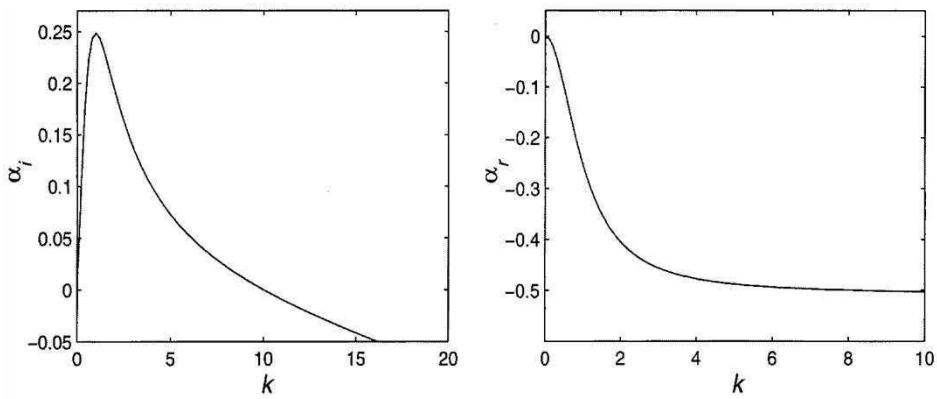

Figure 2. Frequency α_{i} and decay rate α_{r} in the GL model (6) with $\tau_1 = 0.01$, $\tau_2 = 0.005$.

We introduce fields of velocity and rate of change of temperature as

$$v = \frac{\partial u}{\partial t} \qquad q = \frac{\partial \theta}{\partial t}$$

Then we seek the solution to system (19) in the form of the Fourier series

$$\begin{aligned} u &= \sum_{n=-\infty}^{\infty} U_n(t) e^{ink x} & v &= \sum_{n=-\infty}^{\infty} V_n(t) e^{ink x} \\ \theta &= \sum_{n=-\infty}^{\infty} \Theta_n(t) e^{ink x} & q &= \sum_{n=-\infty}^{\infty} Q_n(t) e^{ink x} \end{aligned} \tag{20}$$

Substituting Eqs. (20) into system (19) and equating coefficients of $\exp(inkx)$ lead to an infinite system of coupled ordinary differential equations for the amplitudes of the Fourier modes

$$\begin{aligned} \frac{dU_n}{dt} &= V_n \\ \frac{dV_n}{dt} &= -(nk)^2 U_n - 2\gamma i k^2 \sum_{m=-\infty}^{\infty} m(n-m)^2 U_m U_{n-m} \\ &\quad + 3\delta k^4 \sum_{m,l=-\infty}^{\infty} ml(n-m-l)^2 U_m U_l U_{n-m-l} \\ &\quad + \beta_1 ink \Theta_n - \beta_2 k^2 \sum_{m=-\infty}^{\infty} m^2 U_m \Theta_{n-m} \\ &\quad - \beta_2 k^2 \sum_{m=-\infty}^{\infty} m(n-m) U_m \Theta_{n-m} + \beta_1 \tau_1 ink Q_n \\ \frac{d\Theta_n}{dt} &= Q_n \\ \frac{\tau_2 dQ_n}{dt} &= -Q_n + aink V_n - bk^2 \sum_{m=-\infty}^{\infty} m(n-m) U_m V_{n-m} \\ &\quad - \alpha k^3 i \sum_{m=-\infty}^{\infty} m^2 (n-m) U_m \Theta_{n-m} - k^2 n^2 \Theta_n \\ &\quad - \alpha k^3 i \sum_{m=-\infty}^{\infty} m(n-m)^2 U_m \Theta_{n-m} \end{aligned} \tag{21}$$

The system (21) was truncated to a finite number of modes, typically 32, and integrated in time using the fourth-order Runge–Kutta method.

Before proceeding to the study of the thermomechanical system, we conducted some numerical tests. In particular, we made sure that the numerical code well reproduced an exact traveling wave solution of the linearized system (19) with

$\beta_1 = \gamma = \delta = \beta_2 = b = \alpha = 0,\ a \neq 0$

$$u = A\sin(k(x-t))$$
$$\theta = \frac{(1-\tau_2)aAk^2}{(1-\tau_2)^2k^2+1}\sin(k(x-t)) + \frac{aAk}{(1-\tau_2)^2k^2+1}\cos(k(x-t)) \qquad (22)$$

Figure 3, where both the numerical solution and exact solution (22) for $A = 10.0$, $a = -0.926$, $k = 0.05$, $\tau_2 = 0.005$ are presented, confirms that there is practically no discrepancy between the numerical and exact solutions. We exploit Eqs. (22) to set the initial conditions for our nonlinear problem.

Strictly speaking the parameters β_1 and a must equal or not equal zero simultaneously; see Eqs. (5). But the example for steel in the second section shows that the value β_1 is relatively small and the respective term can be neglected (note that a similar assumption was applied in [14] where, however, no relaxation time was taken into account).

A number of other tests were also conducted to ensure that the numerical code correctly allows for the nonlinear terms. Specifically, Eqs. (19) were supplied by forcing functions $f(x,t)$ and $g(x,t)$ that provide a prescribed analytic form for the solution. Then the analytic and numerical solutions were compared with each other. For example, a test was performed with the exact solution $u = (1 + A/N\ \sin(kx-\omega t))^N$, $\theta = C\ \cos(kx-\omega t)$ for constant integer N and real constants A and ω. Having substituted these expressions into system (19) we calculated the necessary forcing functions f and g. Note that the cubic nonlinearity in system (19) generates $3N$ modes after decomposition into the Fourier series. Consequently, the functions $f(x,t)$ and $g(x,t)$ are quite cumbersome even for the case $N = 3$, being composed of $3N = 9$ modes. Since we have both cosines and sines in the series, this gives 18 terms. The exact and numerical solutions in the tests coincided no worse than in the preceding example for the linear wave (22).

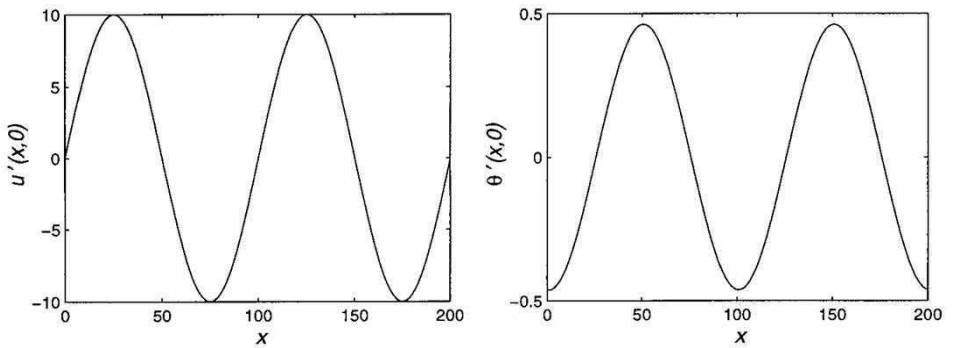

Figure 3. The wave (22) provides initial conditions for the nonlinear problem.

Our first task is to observe how the shape of the wave (22) transforms with time as the amplitude A is increased and, consequently, the nonlinear effects become more important. We should bear in mind that the set of initial conditions also includes initial values of time derivatives of temperature and of displacement. We assume these initial values change proportionally to the initial amplitudes from experiment to experiment.

It is convenient to scale displacement and temperature so that their scaled values satisfy the same initial conditions. The scaled variables u' and θ' are defined as $u = \varepsilon u'$, $\theta = \varepsilon\theta'$, where ε is a positive factor. This leads to the system for u' and θ'

$$\begin{cases} \dfrac{\partial^2 u'}{\partial t^2} - \dfrac{\partial^2 u'}{\partial x^2}\left(1 + 2\gamma\varepsilon\dfrac{\partial u'}{\partial x} + 3\delta\varepsilon^2\left(\dfrac{\partial u'}{\partial x}\right)^2\right) \\ \qquad - \beta_1\dfrac{\partial\theta'}{\partial x} - \beta_1\tau_1\dfrac{\partial^2\theta'}{\partial x\partial t} - \beta_2\varepsilon\dfrac{\partial}{\partial x}\left(\dfrac{\partial u'}{\partial x}\theta'\right) = 0 \\ \tau_2\dfrac{\partial^2\theta'}{\partial t^2} + \dfrac{\partial}{\partial t}\left(\theta' - a\dfrac{\partial u'}{\partial x} - \dfrac{1}{2}b\varepsilon\left(\dfrac{\partial u'}{\partial x}\right)^2\right) - \dfrac{\partial}{\partial x}\left(\left(1 + \alpha\varepsilon\dfrac{\partial u'}{\partial x}\right)\dfrac{\partial\theta'}{\partial x}\right) = 0 \end{cases} \tag{23}$$

The systems (19) and (23) differ only in the values of the coefficients. As is evident from system (23), the scaled coefficients that we mark by primes are

$$\gamma' = \varepsilon\gamma \qquad \delta' = \varepsilon^2\delta \qquad \beta_1' = \beta_1 \qquad \beta_2' = \varepsilon\beta_2 \qquad a' = a \qquad b' = \varepsilon b \qquad \alpha' = \varepsilon\alpha$$

If ε is infinitely small, then the nonlinear terms in system (23) are negligible compared to the linear terms and, in the zero-order approximation in ε, we recover the linear system.

The linear system (23) has an exact solution (22) in which u and θ should be replaced by u' and θ'. This solution obviously represents a wave that keeps its shape. This fact makes such a wave an attractive candidate for the initial conditions in our nonlinear problem. Thus, our initial conditions are chosen to be

$$\begin{aligned} u'(x,0) &= A\sin(kx) \\ \theta'(x,0) &= \frac{(1-\tau_2)aAk^2}{(1-\tau_2)^2k^2+1}\sin(kx) + \frac{aAk}{(1-\tau_2)^2k^2+1}\cos(kx) \\ \left(\frac{\partial u'}{\partial t}\right)_{t=0} &= -Ak\cos(kx) \\ \left(\frac{\partial\theta'}{\partial t}\right)_{t=0} &= -\frac{(1-\tau_2)aAk^3}{(1-\tau_2)^2k^2+1}\cos(kx) + \frac{aAk^2}{(1-\tau_2)^2k^2+1}\sin(kx) \end{aligned}$$

In the course of the numerical experiments we will demonstrate how the sinusoidal wave is deformed by the nonlinearities. Any alterations in ε not only lead to a change in the initial amplitudes of (u, θ) but also to a proportional change in their time derivatives. Thus, depending on the magnitude of ε we obtain a range of initial conditions for our problem in terms of (u, θ). By increasing ε, we amplify the influence of nonlinearities in the system (23).

It is well known that large-amplitude (nonlinear) waves degenerate into nonsmooth solutions [31, 32]. As is demonstrated by Eqs. (22) this is not the case for the small-amplitude (linear) wave. Now we take into account that β_1 is not exactly zero, albeit small. Then the actual linear solution starting from the profile (22) decays, not to mention that no singularity emerges. Because β_1 is nonzero, it does participate in the linearized model and is more significant than the nonlinear terms, which can always be made infinitesimal by making ε sufficiently small. The coefficient β_1 has its effect over a sufficiently long period of time, causing the wave to decay slowly. Thus, the steady wave (22) should be considered an approximation of the actual decaying solution considered in the second section.

For sufficiently large values of ε, the nonlinearities come into action dominating over the linear terms and leading to the formation of discontinuity. To demonstrate the nonlinear effects we present the solution of system (23) in the form of three-dimensional graphs showing the time evolution of the whole spatial profiles of displacement and temperature. The two-dimensional plot near each three-dimensional plot shows the profile at some moment t_* when the computational experiment was stopped. If the experiment was continued, the profiles would become rippled, indicating that the number of modes (32 in our work) is no longer sufficient to represent the solution accurately. For visual convenience, we plot two periods of the profiles. Thus, left-, middle-, and right-hand points of each graph correspond to the same physical point. The coefficients near the linear terms we used for the computations were $a = -0.926$ and $\beta_1 = -5.035 \times 10^{-3}$, which are typical nondimensional coefficients for steel (see the second section). The rest of the coefficients were scaled, respectively, from data presented in [14]: $\gamma = 1.0$, $\delta = 0.5$, $\beta_2 = 0.001$, $b = 0.1$, $\alpha = 1.0$. Results, with the wave number $k = 0.05$ are obtained using 32 Fourier modes.

First we present (Figures 4 to 6) the dynamics of the thermoelastic rod under different degrees of nonlinearity and fixed relaxation times $\tau_1 = \tau_2 = \tau = 0.005$. Figure 4 ($\varepsilon = 1$) demonstrates a sharpening of certain sections of the displacement and temperature profiles caused by nonlinearities. Thus, both profiles gradually approach nonsmooth forms with discontinuous derivatives. Starting from sinusoidal waves shown in Figure 3, the displacement and temperature distributions are transformed into distinctly different shapes according to the laws governing their coupled dynamics. Figure 5 ($\varepsilon = 5.0$) and Figure 6 ($\varepsilon = 15.0$) demonstrate the increasing influence of nonlinearities. We observe that the dynamics are characterized by the splitting of the peak of the temperature profile and almost a triangular shape of the displacement profile. We emphasize that, with the nonlinear effects coming into play, the solution approaches the nonsmooth form faster. Consequently, we have to shorten the numerical experiment by decreasing the limiting time t_*.

Our second group of nonlinear computations concerns the influence of the relaxation time on the nonlinear dynamics of the thermoelastic body. The range of reported values of the relaxation time for different materials is quite wide: $t_0 = (10^{-15} - 10^{-10})$ sec [2]. When going from material to material, not only do τ, τ_1, and τ_2 change but so also do all the other coefficients of the thermoelastic equations. Regrettably, among those, only the values of the coefficients near the linear terms are well tabulated in literature and no reliable data is available on

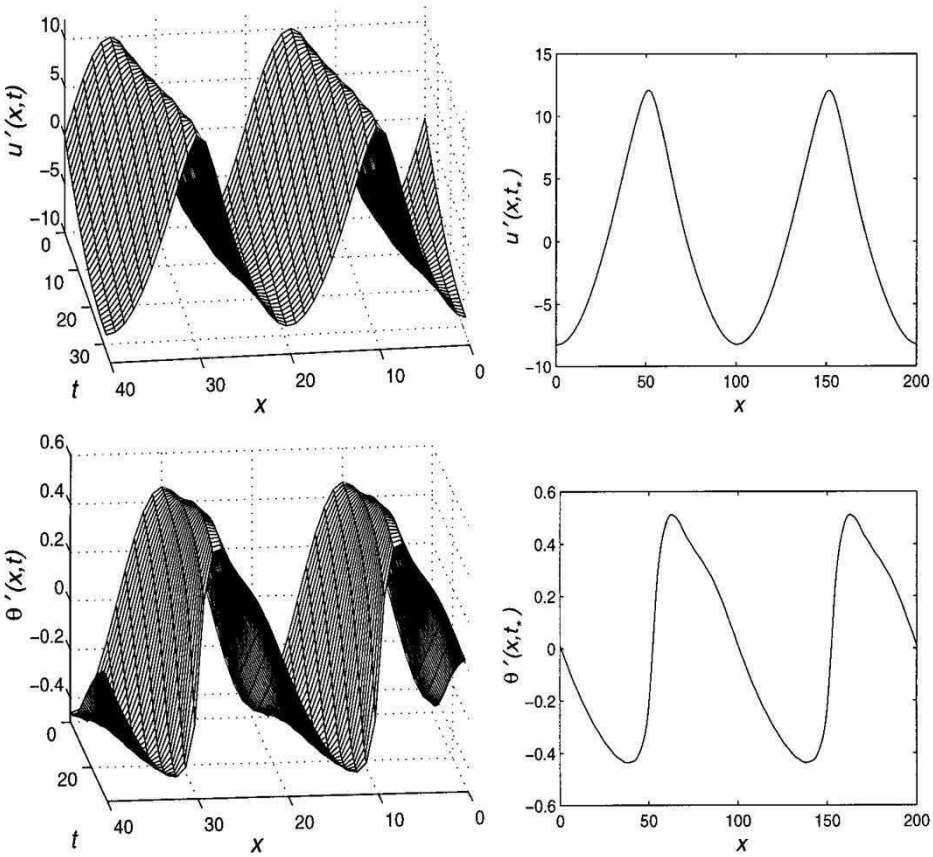

Figure 4. Displacement and temperature dynamics in the weakly nonlinear case $\varepsilon = 1.0$.

the coefficients of the nonlinear terms. With this in mind, we explored how the relaxation time affects the solution provided that the rest of the parameters are fixed. The initial conditions for this series of computations were again taken in the form shown in Figure 3. After nondimensionalizing based on the characteristics of steel, the preceding interval for t_0 converts into $\tau = 5 \times 10^{-3} - 5 \times 10^2$. In this series of numerical experiments we adopted $\tau_1 = \tau_2 = \tau$ and used fixed $\varepsilon = 1$.

It should be stressed that, once the nonlinear effects produce discontinuous solutions, the relaxation time should be inevitably important in the areas where the discontinuity is about to form. However, because of computational difficulties we are unable to approach this situation very closely. In order to see what qualitative consequences may arise from the effect of the thermal relaxation we modeled a somewhat artificial, atypical for metals, situation using extremely large values of the relaxation time $\tau = 5$ and $\tau = 500$.

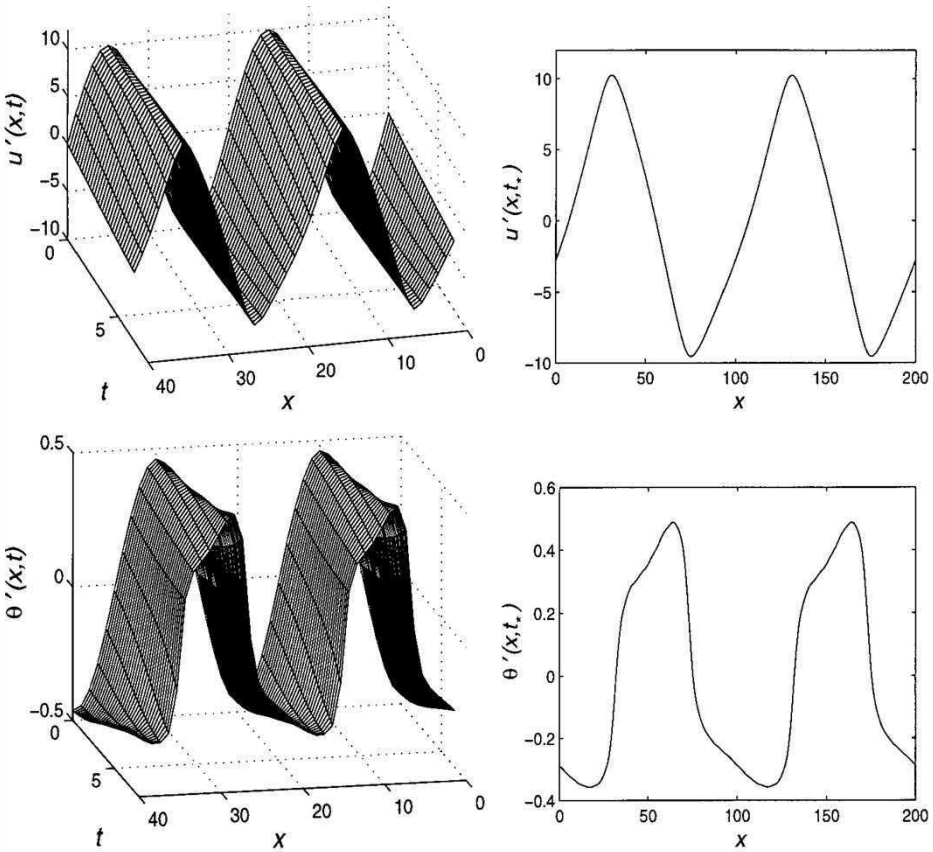

Figure 5. Displacement and temperature dynamics in the moderately nonlinear case $\varepsilon = 5.0$.

Figure 7 shows the profiles of displacement and temperature at the moment $t_* = 32.5$ in the experiment with moderate relaxation time $\tau = 5.0$. There are minor differences between these profiles and the profiles at the same moment of time in Figure 4, where $\tau = 0.005$. But for a much larger relaxation time $\tau = 500.0$ (Figure 8) the temperature profiles are nearly sinusoidal during the whole experiment.

To understand the mechanism controlling the dynamics in these sets of experiments (for different degrees of nonlinearity and different relaxation times) we estimate the terms included in system (23). We start with the equation of motion. Denoting the absolute values of typical variations of u', θ', t, x by U, Θ, T, and X, respectively, we have, by the order of magnitudes,

$$\left|\frac{\partial^2 u'}{\partial t^2}\right| \sim \frac{U}{T^2} \tag{24}$$

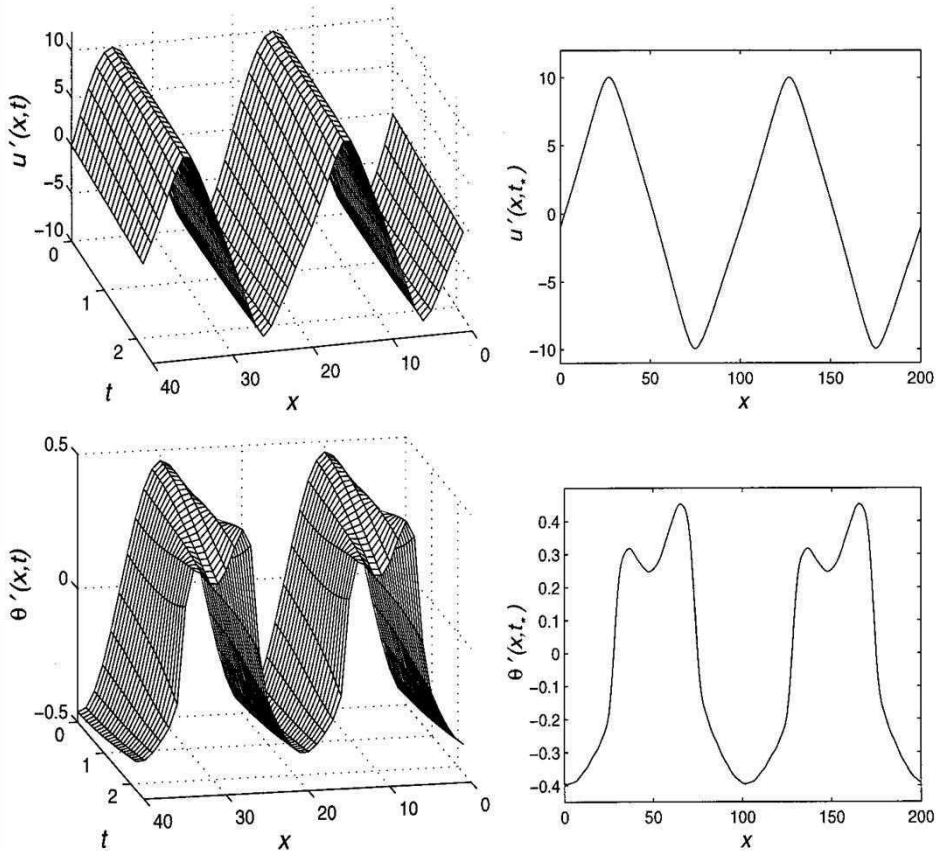

Figure 6. Displacement and temperature dynamics in the strongly nonlinear case $\varepsilon = 15.0$.

The estimates of the nonlinear terms are

$$2\gamma\varepsilon\left|\frac{\partial^2 u'}{\partial x^2}\,\frac{\partial u'}{\partial x}\right| \sim 2\gamma\varepsilon\frac{U^2}{X^3} \qquad 3\delta\varepsilon^2\left|\frac{\partial^2 u'}{\partial x^2}\right|\left(\frac{\partial u'}{\partial x}\right)^2 \sim 3\delta\varepsilon^2\frac{U^3}{X^4}$$
$$\beta_2\varepsilon\left|\frac{\partial}{\partial x}\left(\frac{\partial u'}{\partial x}\theta'\right)\right| \sim \beta_2\varepsilon\frac{U\Theta}{X^2} \tag{25}$$

Equating Eqs. (24) and (25) by the order of magnitude, we find typical time intervals required by the terms (25) to produce a perceptible effect on the displacement dynamics (we label the respective values of T by the coefficient character corresponding to the given nonlinear term)

$$T_\gamma \sim \left(\frac{X^3}{2\gamma\varepsilon U}\right)^{1/2} \qquad T_\delta \sim \frac{X^2}{U\varepsilon(3\delta)^{1/2}} \qquad T_\beta \sim \frac{X}{(\beta_2\varepsilon\Theta)^{1/2}} \tag{26}$$

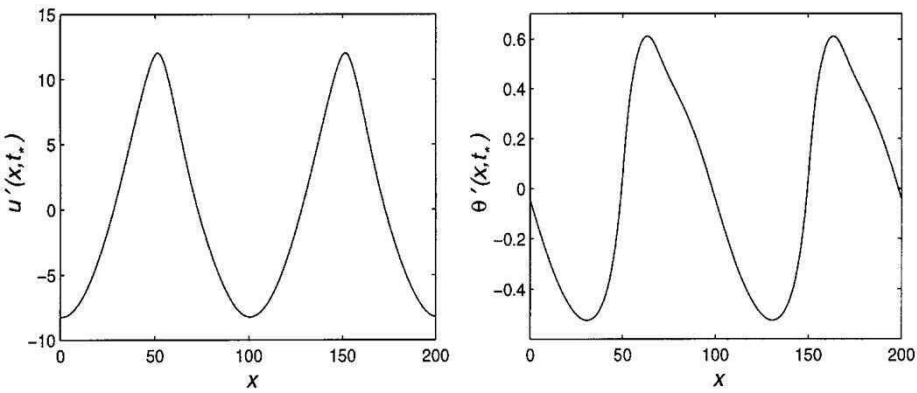

Figure 7. Displacement and temperature formed by the moment t_* for moderate relaxation time $\tau = 5$.

Typical variations of displacement and temperature were $U \sim 20$, $\Theta \sim 1$. The scale X is estimated as a half of the wave length, that is

$$X \sim \frac{\pi}{k} \tag{27}$$

Then substituting the used magnitudes of the constants into Eqs. (26) and (27) we obtain for $\varepsilon = 1$: $T_\gamma \sim 70$, $T_\delta \sim 150$, $T_\beta \sim 2000$; for $\varepsilon = 5$: $T_\gamma \sim 30$, $T_\delta \sim 30$, $T_\beta \sim 850$; ~ 850; and for $\varepsilon = 15$: $T_\gamma \sim 20$, $T_\delta \sim 10$, $T_\beta \sim 500$. These values may also serve as rough estimates of the moments of the discontinuity formation. The durations of the numerical experiments were $t_* = 32.5$, 6.8, 2.3, respectively. We see that t_* is significantly less than T_γ, T_δ, and T_β; that is, the experiments were stopped well before those moments. However, the analysis here is only qualitative. Obviously the terms leading to a shorter typical time act faster. Because $T_\beta \gg t_*$, the third of Eqs. (25) is negligible in all three cases $\varepsilon = 1$, 5, 15. In the case $\varepsilon = 1$, we have $t_* \sim T_\gamma < T_\delta \ll T_\beta$, implying that the first of Eqs. (25) is the prevailing nonlinearity. For the case $\varepsilon = 5$, $T_\gamma \sim T_\delta \ll T_\beta$ and, thus, the first and second equations of (25) are both important. For the case $\varepsilon = 15$: $T_\delta < T_\gamma \ll T_\beta$, and, thus, the prevailing term is the second of Eqs. (25). Finally it can be easily shown that the terms with the coefficient β_1 are extremely small and thus play an insignificant role in the dynamics. Therefore, displacement in the presented experiments is practically decoupled from temperature (while temperature, as we will see, essentially depends on displacement) and subjected to the displacement-only-associated nonlinearities.

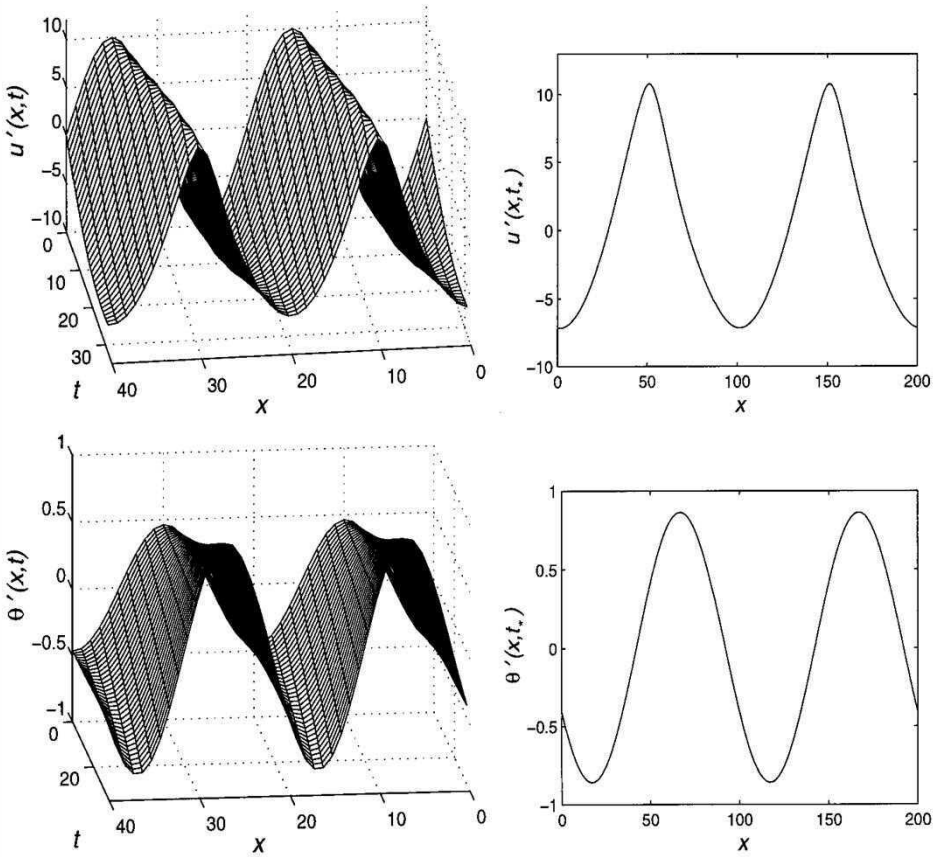

Figure 8. Displacement and temperature dynamics for large relaxation time $\tau = 500$.

Now consider the energy balance equation. We have the estimates

$$\tau_2\left|\frac{\partial^2\theta'}{\partial t^2}\right| \sim \frac{\tau_2\Theta}{T^2} \qquad \left|\frac{\partial\theta'}{\partial t}\right| \sim \frac{\Theta}{T}$$
$$a\left|\frac{\partial^2 u'}{\partial t\partial x}\right| \sim \frac{aU}{TX} \qquad \frac{1}{2}b\varepsilon\left|\frac{\partial}{\partial t}\left(\frac{\partial u'}{\partial x}\right)^2\right| \sim \frac{b\varepsilon U^2}{2TX^2}$$
$$\alpha\varepsilon\left|\frac{\partial}{\partial x}\left(\frac{\partial u'}{\partial x}\,\frac{\partial\theta'}{\partial x}\right)\right| \sim \frac{\alpha\varepsilon U\Theta}{X^3} \tag{28}$$

The terms $\tau_2|\partial_t^2\theta'|$ and $|\partial_t\theta'|$ have the same order provided that $T \sim \tau_2$. This simple relation implies (in agreement with the very sense of the relaxation time) that if the dynamics are slow so that its typical time scale is much larger than τ_2, the relaxation term is negligible in comparison to $\partial_t\theta'$. This was just the case in the experiments with $\tau_2 = 0.005$, where the typical time of the process was $T \sim t_* = 32.5$.

Hence, the typical times produced by different terms of the energy balance equation should be obtained by equating (by the order of magnitude) these terms to $|\partial_t \theta'|$. Doing so with the third of Eqs. (28) we find

$$T_\alpha \sim \frac{X^3}{\alpha \varepsilon U} \tag{29}$$

When doing the same with the second of Eqs. (28) the corresponding typical time cancels and thus cannot be determined. Instead we compare the orders of this term and $|\partial_t \theta'|$. It turns out that the nonlinear term is about 5 times smaller than $|\partial_t \theta'|$ in the case $\varepsilon = 15$ and even smaller in the cases $\varepsilon = 5$ and $\varepsilon = 1$. Therefore, the second of Eqs. (28) may have some influence in the case $\varepsilon = 15$ but has a small effect for $\varepsilon = 5$ and $\varepsilon = 1$. Substituting the parameter values into Eq. (29) we find, respectively, for $\varepsilon = 1, 5, 15$: $T_\alpha \sim 10000, 2100, 700$. Hence, the third of Eqs. (28) is insignificant. From these estimates it follows that the distortion of the temperature profile from sinusoidal should be caused by the first term of Eqs. (28), that is, by the linear displacement-related term. We check this by comparing this term and $|\partial_t \theta'|$, giving

$$\Theta \sim \frac{aU}{X}$$

After inserting the magnitudes, this relation is written as $0.5 \sim 0.5$.

Now consider the experiments with different relaxation times. In the case $\tau = 0.005$ temperature relaxes very quickly; therefore, the regime shown in Figure 4 practically coincides with the regime that would occur if we let $\tau = 0$. At $\tau = 5$ the relaxation period is 6 times shorter than the typical time scale of the process. As a result, we obtained only a small alteration of temperature profile as compared to the previous case. In the case $\tau = 500$ the relaxation period is more than one order longer than the duration of the experiment. Comparing Figure 8 and Figure 4 clearly shows that the larger relaxation time provides a "smoother" (i.e., characterized by a smaller typical magnitude of spatial derivative) profile of temperature formed in the same moment of time.

To give a plausible explanation of this effect, recall that one of the major consequences of the relaxation time is a faster (when τ is small) or slower (when τ is large) relaxation of a system to a certain regime. In our system, we deal with the regime characterized by discontinuity in the solution or its derivatives. For larger τ, we have longer transitions from the sinusoidal wave to the nonsmooth regimes. Moreover, Figure 8 shows a situation where a large value of τ makes the transition extremely long, so no sign of discontinuity formation is observed during the numerical experiment. However, this does not rule out that the discontinuity will appear at a later moment of the dynamics.

CONCLUSIONS

In this article we analyzed linear and nonlinear thermoelastic waves propagating in an infinite rod using models with relaxation times. Carrying out spectral analysis of the Lord–Schulman and Green–Lindsay linear models, we derived dependencies of decay rates and frequency shifts of temperature and displacement upon the wave number. Short disturbances of displacement and temperature were shown to decay at a constant rate. Results for the LS and GL models coincide, provided the values of the two relaxation times in the GL model equal the value of relaxation time in the LS model. A series of numerical experiments was carried out with a general nonlinear model to show the evolution of initially harmonic profiles of displacement and temperature. The influence of different nonlinear terms on the dynamics was thoroughly analyzed. Studying the combined effect of relaxation time and nonlinearities, we demonstrated and interpreted experiments where a large relaxation time prevents the formation of a nonsmooth temperature profile by the time this would occur if relaxation time is small.

REFERENCES

1. I. Muller and T. Ruggeri, *Extended Thermodynamics*, Springer-Verlag, New York, 1993.
2. D. S. Chandrasekharaiah, Thermoelasticity with Second Sound: a Review, *Appl. Mech. Rev.*, vol. 39, pp. 355–376, 1986.
3. B. D. Coleman and D. C. Newman, Implications of a Nonlinearity in the Theory of Second Sound in Solids, *Phys. Rev. B*, vol. 37, pp. 1492–1498, 1988.
4. T. Ruggeri, A. Muracchini, and L. Seccia, Shock Waves and Second Sound in a Rigid Heat Conductor: a Critical Temperature for NaF and Bi, *Phys. Rev. Lett.*, vol. 64, pp. 2640–2643, 1990.
5. D. S. Chandrasekharaiah, Hyperbolic Thermoelasticity: a Review of Recent Literature, *Appl. Mech. Rev.*, vol. 51, pp. 705–729, 1998.
6. R. B. Hetnarski and J. Ignaczak, Soliton-like Waves in a Low-temperature Nonlinear Thermoelastic Solid, *Int. J. Engng. Sci.*, vol. 34, pp. 1767–1787, 1996.
7. R. B. Hetnarski and J. Ignaczak, On Soliton-like Thermoelastic Waves, *Appl. Anal.*, vol. 65, pp. 183–204, 1997.
8. R. V. N. Melnik, Steklov's Operator Technique in Coupled Dynamic Thermoelasticity, in R. W. Lewis and J. T. Cross (Eds.), *Numerical Methods in Thermal Problems*, Vol. X, pp. 139–150, 1997.
9. K. Saxton, R. Saxton, and W. Kosinski, On Second Sound at the Critical Temperature, *Quart. Appl. Math.*, vol. LVII, pp. 723–740, 1999.
10. W. Dreyer and M. Kunik, Initial and Boundary Value Problems of Hyperbolic Heat Conduction, *Continuum Mech. Thermodyn.*, vol. 4, pp. 227–245, 1990.
11. J. Ignaczak, Soliton-like Solutions in a Nonlinear Dynamic Coupled Thermoelasticity, *J. Thermal Stresses*, vol. 13, pp. 73–98, 1990.
12. T. S. Öncu and T. B. Moodie, On the Constitutive Relations for Second Sound in Elastic Solids, *Arch. Rat. Mech. Anal.*, vol. 121, pp. 87–99, 1992.
13. C. S. Suh and C. P. Burger, Effects of Thermomechanical Coupling and Relaxation Times on Wave Spectrum in Dynamic Theory of Generalized Thermoelasticity, *J. Appl. Mech.*, vol. 65, pp. 605–613, 1998.
14. A. N. Abd-alla, A. F. Ghaleb, and G. A. Maugin, Harmonic Wave Generation in Nonlinear Thermoelasticity, *Int. J. Engrg. Sci.*, vol. 32, pp. 1103–1116, 1994.
15. E. K. Rawy, L. Iskandar, and A. F. Ghaleb, Numerical Solution of a Nonlinear, One-dimensional Problem of Thermoelasticity, *J. Comput. Appl. Math.*, vol. 100, pp. 53–76, 1998.

16. P. D. Lax, Development of Singularities of Solutions of Nonlinear Differential Equations, *J. Math. Phys.*, vol. 5, pp. 611–613, 1964.
17. R. C. MacCamy and V. J. Mizel, Existence and Non-existence in the Large of Solutions of Quasilinear Wave Equations, *Arch. Rat. Mech. Anal.*, vol. 25, pp. 299–320, 1967.
18. M. Slemrod, Global Existence, Uniqueness, and Asymptotic Stability of Classical Smooth Solutions in One-dimensional Non-linear Thermoelasticity, *Arch. Rat. Mech. Anal.*, vol. 76, pp. 97–133, 1981.
19. H. W. Lord and Y. Schulman, A Generalized Dynamic Theory of Thermoelasticity, *J. Mech. Phys. Solids*, vol. 15, pp. 299–309, 1967.
20. A. E. Green and K. E. Lindsay, Thermoelasticity, *J. Elasticity*, vol. 2, pp. 1–7, 1972.
21. L. Kowalski, Existence and Uniqueness of the Solution of the First Boundary-Initial Value Problem for Linear Hyperbolic Thermoelasticity Equations, *Ann. Soc. Math. Polon. Ser. I: Comment. Math.*, vol. 33, pp. 73–79, 1993.
22. J. Gawinecki, Initial-Boundary Value Problems in Linear and Nonlinear Hyperbolic Thermoelasticity Theory, *Z. Angew. Math. Mech.*, vol. 78, pp. S911–S912, 1998.
23. J. H. Prevost and D. Tao, Finite Element Analysis of Dynamic Coupled Thermoelasticity Problems with Relaxation Times, *J. Appl. Mech.*, vol. 50, pp. 817–822, 1983.
24. D. E. Glass and K. K. Tamma, Non-Fourier Dynamic Thermoelasticity with Temperature-Dependent Thermal Properties, *J. Thermophys. Heat Transfer*, vol. 8, pp. 145–151, 1991.
25. W. Nowacki, *Thermoelasticity* , Pergamon, Oxford, 1962.
26. V. V. Novozhilov, *Foundations of the Nonlinear Theory of Elasticity*, Graylock Press, Rochester, NY, 1953.
27. S. Antman, *Nonlinear Problems of Elasticity*, Springer, NY, 1994.
28. R. S. Manning, J. H. Maddocks, and J. D. Kahn, A Continuum Rod Model of Sequence-Dependent DNA Structure, *J. Chem. Phys.*, vol. 105, pp. 5626–5635, 1996.
29. J. Miklowitz, *The Theory of Elastic Waves and Waveguides*, North-Holland, Amsterdam, 1978.
30. L. D. Landau and E. M. Lifshitz, *Theory of Elasticity*, Butterworth-Heinemann, Oxford, 1995.
31. R. Racke, On the Cauchy Problem in Nonlinear 3D-Thermoelasticity, *Math. Z.*, vol. 203, pp. 649–682, 1990.
32. R. Racke, Blow-up in Non-linear Three-dimensional Thermoelasticity, *Math. Methods Appl. Sci.*, vol. 12, pp. 267–273, 1990.